

## Stress-Corrosion Behavior of Magnesium Alloy Az91 Manufactured by Laser Powder Bed Fusion

Chelsea O'Donnell<sup>1</sup>, Alejandro Avila<sup>1</sup>, Bradley Kauffman<sup>1</sup>, Adrian Passinger<sup>1</sup>, Robert Stewart<sup>1</sup>,  
David Scott Fernander<sup>1</sup>, Dina Khattab<sup>2</sup>, Michael Titus<sup>2</sup>, Michael P. Sealy<sup>1\*</sup>

<sup>1</sup> School of Mechanical Engineering, Purdue University, West Lafayette, IN 47907, U.S.A.

<sup>2</sup> School of Materials Engineering, Purdue University, West Lafayette, IN 47907, U.S.A.

### Abstract

This study investigated how laser powder bed fusion (LPBF) processing parameters affect the stress-corrosion behavior of AZ91 magnesium alloy, a lightweight material of interest for aerospace and marine components. The hypothesis was that porosity-driven stress localization accelerates corrosion under tensile stress. LPBF parameters (*i.e.*, laser power and scan speed) were varied to modulate energy density and generate distinct porosity features. Open circuit potential and potentiodynamic polarization tests were conducted under applied tensile load to characterize the corrosion response. Results showed that corrosion rates decreased with build height, with bottom layers exhibiting lower corrosion, suggesting that thermal history and resulting microstructure influence corrosion behavior. Some suboptimal samples exhibited lower corrosion rates under load, contrary to expectations. These trends suggest that both porosity morphology and build height contribute to stress-corrosion behavior in magnesium. This work contributes to AM design frameworks that account for corrosion performance under service-relevant loading.

**Keywords:** Additive manufacturing, Magnesium alloy, Corrosion, Laser powder bed fusion

### 1. Introduction

Additive manufacturing of AZ91 magnesium alloy via LPBF enables the fabrication of lightweight components with complex geometries for aerospace and marine applications. However, AZ91 remains highly susceptible to corrosion and stress-corrosion cracking due to its reactive nature and porosity-prone melt pool dynamics. The combination of high vapor pressure, rapid solidification, and limited wetting behavior in magnesium alloys promotes the formation of gas porosity and lack-of-fusion defects, which serve as both stress concentrators and sites of electrochemical instability.

Prior studies on AM of magnesium alloys have largely focused on process feasibility, basic corrosion behavior, or mechanical strength. Few studies, however, have evaluated the simultaneous effect of tensile stress and electrochemical corrosion in LPBF-processed AZ91. This limits our understanding of how as-built defects and thermal gradients from the LPBF process influence service-life degradation in corrosive environments.

This work aims to fill this gap by systematically analyzing the stress-corrosion response of LPBF-fabricated AZ91 samples subjected to varying energy inputs. Tensile stress was applied during electrochemical testing to simulate service conditions, and trends were correlated with LPBF parameter-induced porosity and build layer location. These results offer insights into designing LPBF components for high-performance structural applications in corrosive environments.

## 2. Literature Review

### 2.1 Magnesium alloy corrosion behavior and additive manufacturing

Magnesium alloys are highly reactive in aqueous environments, particularly chloride-containing solutions, due to their low electrode potential. AZ91, a widely used Mg alloy, exhibits complex corrosion mechanisms that involve microgalvanic coupling between the  $\alpha$ -Mg matrix and intermetallic  $\beta$ -phases [1]. Traditional casting methods have shown that localized corrosion often initiates at grain boundaries or at inclusions, leading to pitting and cracking under stress.

The LPBF process for magnesium alloys introduces unique challenges, such as vaporization, balling, and lack of fusion due to rapid solidification and poor wetting. These defects are difficult to control and can vary significantly with process parameters. Porosity, particularly elongated lack-of-fusion voids, plays a key role in both mechanical degradation and corrosion susceptibility. High-energy densities may reduce porosity but also increase thermal gradients, potentially inducing residual stress. Figure 1 highlights the printability of magnesium alloys as a function of laser power, scan speed, hatch spacing, and layer thickness [2]. The most important parameters affecting the corrosion properties in L-PBF Mg and Al alloys include scan speed, hatch spacing, exposure, and layer size [3]. Through PDP testing, the study showed that to reduce porosity, a larger hatch distance, smaller scan speed, and smaller layer size were optimal. This information was valuable for this research in order to determine the parameters needed to achieve different porosity levels to understand AZ91's corrosion behavior.

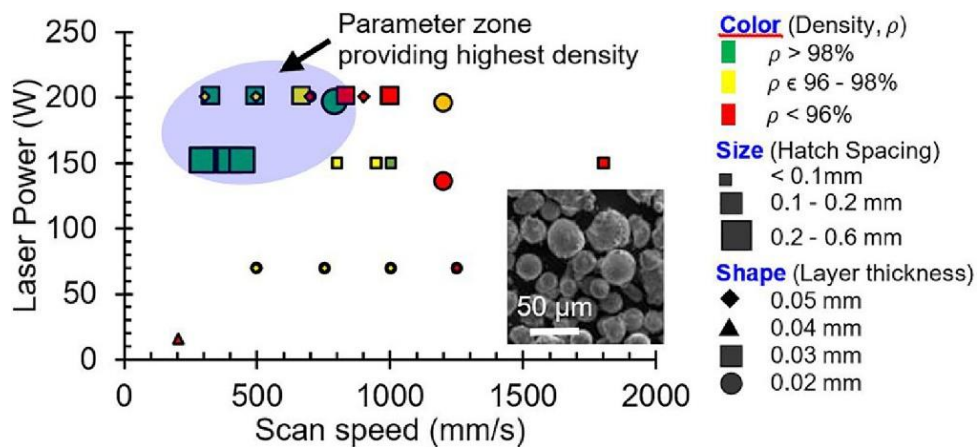


**Figure 1:** Printability of Mg alloys as a function of laser power and scan speed [2].

## 2.2 Stress-corrosion testing

Stress-corrosion cracking (SCC) in Mg alloys has traditionally been studied through slow strain rate tests and cantilever beam methods. Studies have shown that the interaction of stress fields and corrosion pits leads to crack nucleation and propagation. However, there is limited literature combining in-situ electrochemical testing with tensile loading in LPBF-processed Mg. Electrochemical techniques, such as PDP and OCP, can reveal early corrosion activity, but their integration with applied stress remains underexplored for AM materials. A stress-corrosion study on wrought AZ91 magnesium alloy found that the corrosion rate increased as the applied stress increased [4]. The study used four-point bending and discussed the emergence of pits due to the applied stress, which results in higher corrosion. This was relevant for the study since it discusses the effect of material properties, such as grain boundaries, dislocations, and porosity which were varied in this experiment by modifying the L-PBF parameters.

One standard test method for stress-corrosion behavior is ASTM G49 [5]. This standard discusses the reasoning behind the need for stress-corrosion testing and some of the general behavior of non-ferrous metals. The standard was helpful to inform the experimental procedures on how to manufacture the spring-loaded testing setup and how the stress corrosion results need to be reported. This standard is essential since it provides researchers with a toolkit but also ensures that the data is consistent and accurate.

Other previous literature discussed the corrosion behavior of biodegradable magnesium implants and the current testing methodologies and the limitations [6]. The study reviews various corrosion methods along with the advantages and disadvantages of mass loss, hydrogen evolution measurement, pH monitoring, PDP testing, and electrochemical impedance spectroscopy. The most relevant part of this paper is the review of PDP testing since it discusses sample preparation, testing results, possible inconsistencies in testing, PDP curve behavior, cathode and anode kinetics, result experimentation, voltage idea testing, and the effect of current density on corrosion. The paper was extremely relevant since it introduced the importance of integrating open circuit potential (OCP) testing before running PDPs to ensure that results were consistent even with varying samples. Due to the metal having to stabilize when introduced to a salt solution, the OCP test is essential to avoid continuous errors. Finally, the paper discussed the usage of Tafel fits to calculate  $E_{corr}$ ,  $i_{corr}$ , and corrosion values to understand the corrosion behavior of the part. This paper also provided suggestions for scan rates and scan ranges based on the OCP results which were used throughout the testing process.

Few studies have examined the effect of build layer location or the combined influence of porosity and mechanical stress on corrosion in additively manufactured magnesium alloys. Most work considers either microstructure or corrosion in isolation. This study integrates mechanical loading and electrochemical testing to provide a more realistic view of performance degradation in service-relevant environments.

## 3. Experimental Procedure

### 3.1 Laser Powder Bed Fusion

This study investigated the effect of additive manufacturing processes parameters on the corrosion of magnesium AZ91 fabricated via laser powder bed fusion on a 5<sup>th</sup> generation Matsuura Lumex Avance-25 (Figure 2a). The study selected process parameters based on an internally developed machine learning model (Figure 2b). A set of control parameters were selected based on previous experimentally optimal prints as well as findings in literature; high and low values for both the laser power and scan speed were selected for additional samples. The parameters kept constant between samples were the hatch spacing (150  $\mu\text{m}$ ), the layer height (60  $\mu\text{m}$ ), and the spot diameter (80  $\mu\text{m}$ ). The samples were all evenly spaced on a magnesium build plate to minimize the potential for random residual heating between different samples (Figure 3). The scan pattern was  $\pm 45^\circ$ . Five tested samples (the control as well as the altered samples) in addition to four extra research samples were created on the build plate. Table 1 provides the print parameters and were down selected based on theoretical print parameter guide from parallel research at Purdue's Manufacturing and Materials Research Lab (MMRL). Including suboptimal conditions allow for investigating the role of pore formation or other defects on the sensitivity of stress-corrosion behavior.

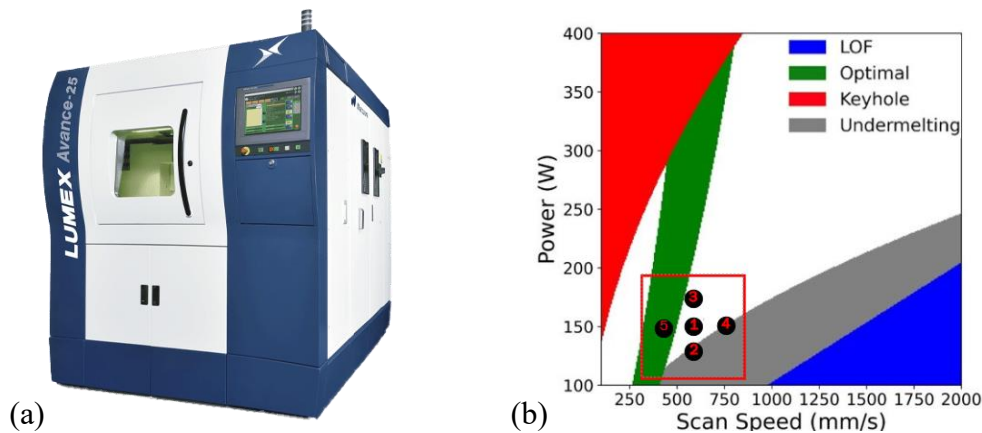


**Figure 2:** (a) Matsuura Lumex Avance-25 hybrid metal LPBF system capable of printing reactive materials and (b) internally developed process parameter map for laser powder bed fusion of magnesium alloy AZ91.

**Table 1:** L-PBF print parameters

Sample Number	Laser Power (W)	Scan Speed (mm/s)
1 – optimized recipe	150	600
2 – lower power	130	600
3 – higher power	170	600
4 – higher speed	150	750
5 – lower speed	150	450

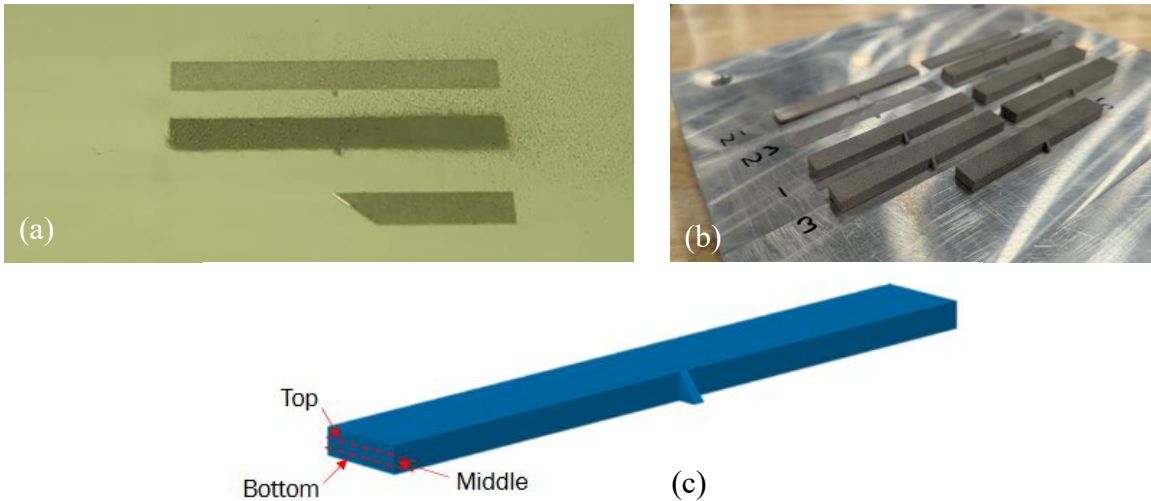


**Figure 3:** Laser powder bed fusion of magnesium alloy AZ91: (a) In-situ printing mid-layer with the laser line visible along the bottom strip; (b) final printed samples on the build plate; and (c) model showing how the sample was wire electric discharge machined to allow testing of three regions with respect to the build direction: top (T), middle (M), and bottom (B).

### 3.2 Stress-Corrosion Testing

#### 3.2.1 Uniaxial tension fixture

Following ASTM G49, a custom uniaxial tension fixture was designed to apply 60 MPa of tensile stress to each sample during corrosion testing. This load was chosen to reduce the likelihood of leaking the solution. Load was held constant using a screw-driven clamp mounted within the electrochemical cell to ensure stable contact during immersion (Figure 4). Each sample was placed in a saline chamber as seen in Figure 5 where a 2% by weight NaCl solution was used for testing.

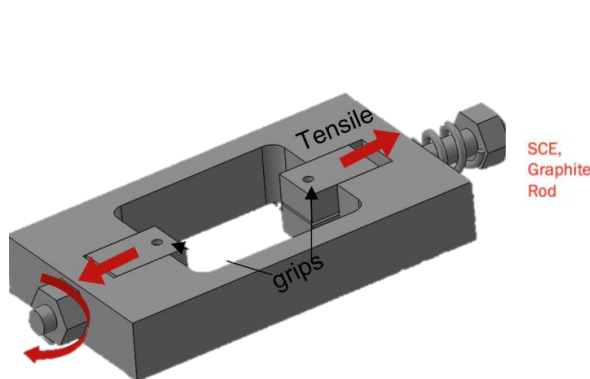


**Figure 4:** Stress-corrosion loading setup.

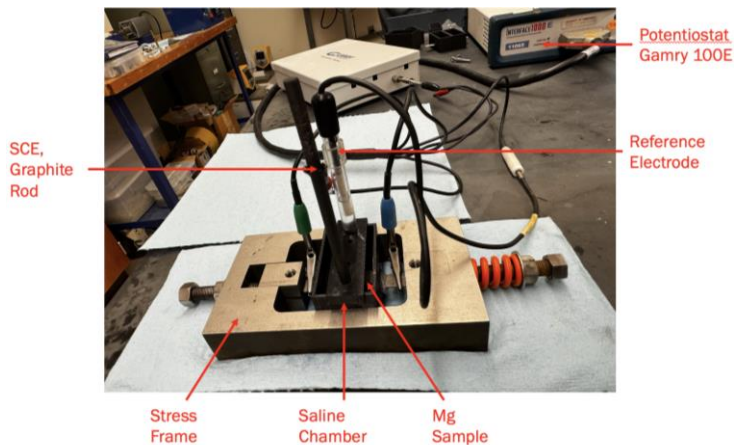


**Figure 5:** Testing for OCP and PDP testing.

### 3.2.2 Electrochemical testing

The polarization method was selected as a comparative analysis tool across additive treatment conditions. Although the immersion test method is more accurate for measuring corrosion rates across magnesium alloys, polarization provides an effective tool for a comparative study on the same alloy. Once the sample was sealed inside the saline chamber, the graphite rod, reference electrode, and Gamry potentiostat were connected to conduct open circuit potential (OCP) and potentiodynamic polarization (PDP) testing. With the potentiostat and sample in place, an OCP test will run until a  $0.1 \text{ Vs}^{-1}$  stabilization is achieved. The time to stabilize was recorded and then an OCP test was conducted for each sample to ensure accurate and consistent results. Next, a PDP test was conducted by defining an appropriate voltage range (-2 V to 1.5 V in this experiment) and a voltage step from  $1 \text{ mVs}^{-1}$  to  $10 \text{ mVs}^{-1}$  was selected depending on the sample properties. Once the unloaded PDP was conducted, the same procedure was repeated to the loaded samples at 60 MPa (*i.e.*, 3 bolt rotations). The same procedure was repeated for each sample and the results are presented in the following sections.

Tafel extrapolation was used to determine corrosion current density ( $i_{corr}$ ) and corrosion potential ( $E_{corr}$ ). The Tafel method is a traditional test of corrosion that neglects mass loss and suggests a linear relation between the corrosion potential and the log of applied current [1]. Tafel curves were calculated from measured PDP data, which is characterized by two diverging lines. The intersection of the two Tafel curves indicates the  $i_{corr}$  or corrosion current, and the equilibrium point of the two PDP reactions indicates the  $E_{corr}$  or the corrosion potential. The corrosion rate is then determined as a function of the current density, molar mass, number of electrons in the reaction, density, and the Faraday constant as given by Equation 1. The imbedded Gamry Tafel Extrapolation tool was implemented to determine the  $E_{corr}$ ,  $i_{corr}$ , and corrosion rates of each sample. Starting and ending points for the Tafel test along the anodic and cathodic curves were selected to include at least one decade of data while excluding data after the sample had oxidized.

$$CR = \frac{K \cdot i_{corr} \cdot EW}{\rho} \quad (1)$$

where:  $CR$  = corrosion rate (*e.g.*, mm/year or mpy [mils per year])

$K$  = unit conversion constant

$i_{corr}$  = corrosion current density ( $\text{A}/\text{cm}^2$ )

$EW$  = equivalent weight of the corroding metal ( $\text{g}/\text{equivalent}$ ), defined as the molar mass ( $\text{g}/\text{mol}$ ) divided by number of electrons exchanged in the anodic reaction

$\rho$  = density of the material

## 4. Results

The results for the OCP testing, the PDP test results for the unloaded and loaded tests, as well as the results for the different regions of the top, middle, and bottom layers are provide in Figures 6-8. All tables with results display the averaged values between either the three regions for the sample-specific analysis or the five samples per layer for the region-based analysis. All results for OCP were based on a run time of 850 seconds to allow each sample to be

electrochemically stable. Finally, all results for corrosion are based on Tafel testing the same way per data set to ensure consistency.

#### 4.1 Open Circuit Potential (OCP)

To start each test, OCP was ran on each of the fifteen samples for 850 seconds to ensure that each sample was electrochemically stable for PDP testing. This was done to ensure the consistency of the results below with the fifteen different samples. Shown below in Figure 6 is a graph of OCP that was conducted for sample 1 with its top, middle, and bottom layer.

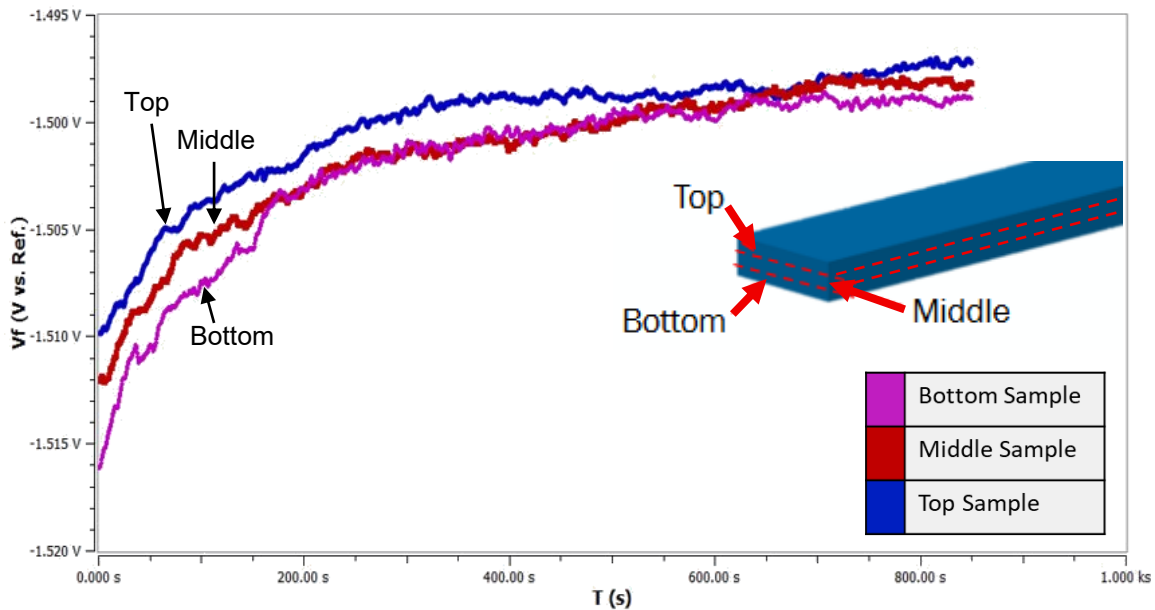


**Figure 6:** OCP test results for the top (blue), middle (red), and bottom (purple) layers for sample 1. Each test ran for a time of 850 seconds.

All other samples had very similar OCP graphs. Each sample reached a  $-0.01$  V stabilization at  $-1.5$  V at approximately 800 seconds. The top layers tended to start with a higher  $V_f$  at the start of the test, while bottom layers started with the lower  $V_f$  values. A reason for this is due to the difference in microstructure from the layers during the PBF printing process. As the bottom layer is printed first, it undergoes more thermal cycling than the subsequent layers which alter its grain structure and make it more electrochemically reactive, leading it to have a larger slope to achieve stability.

#### 4.2 Effect of Loading on Corrosion Behavior

After OCP was completed, each sample was then PDP tested with no load and was immediately tensioned and re-tested with no OCP between the two PDP tests. The goal of testing the sample both unloaded and loaded in a small amount of time was to gather the  $E_{corr}$ ,  $i_{corr}$ , and

corrosion rate data before the corrosion could change the sample's structural integrity or surface finish. It should be noted that this is a limitation of the experiment design. The expectation for the  $E_{corr}$  and  $i_{corr}$  data was to see a shift to the right in  $i_{corr}$  when loaded, which shows that the sample corrodes more under tension and little to no shift in the  $E_{corr}$  value. Figure 7 below shows a sample being PDP tested unloaded and loaded. The PDP tests should shift to the right when comparing the unloaded test to the loaded test for a given sample; however, this was the only sample that this was observed. In samples 2-5, the data showed that when loaded, the  $i_{corr}$  shifted to the left causing a decrease in corrosion which was not expected based on the hypothesis.

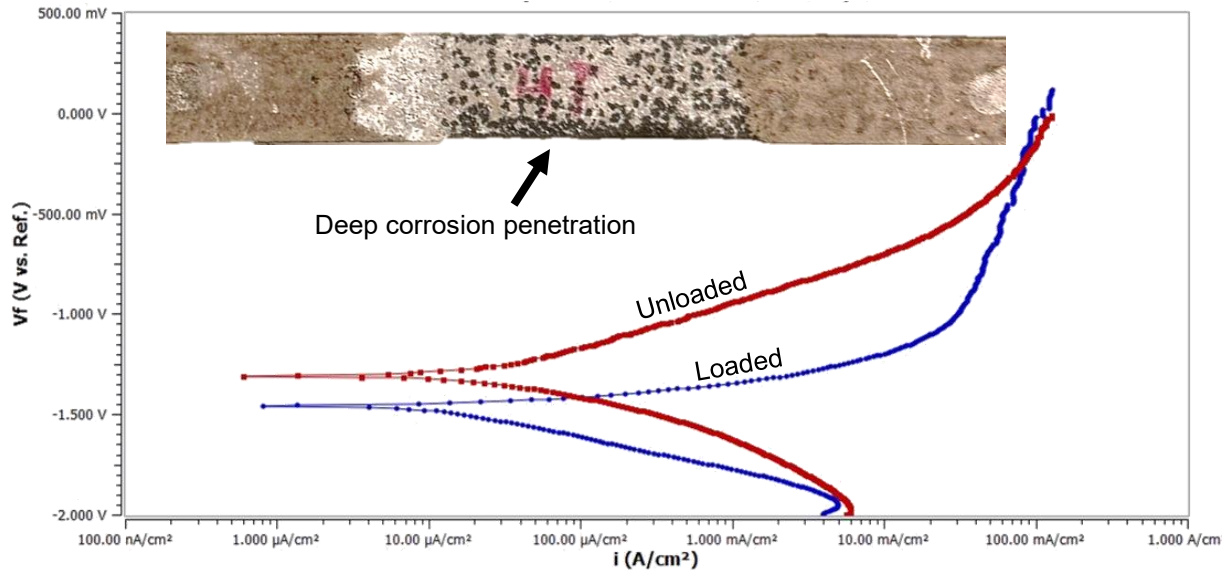


**Figure 7:** Potentiodynamic polarization curves for the top layer of sample 1: unloaded (red) and loaded (blue).

### 4.3 Effect of Laser Power and Scan Speed

The unloaded and loaded data shown in Figures 8 was collected directly after OCP, which means the sample was electrochemically stable for the test every time. The reasoning behind taking an unloaded test first was to show how the graph shifted once the sample was tested when loaded to spot key differences in how the parameters alter the corrosion on a given AZ91 sample. In Figure 8a, PDP tests were run for the bottom layers of samples 1-5 when unloaded. In addition, Table 2 displays the averaged  $E_{corr}$ ,  $i_{corr}$ , and corrosion rate for all five samples in unloaded testing.

The loaded tests were continued directly after the unloaded tests where some samples were already aggressively corroded and is likely a source of experimental error and is a limitation of this methodology. Although the magnitude of data points for these tests may not be fully accurate, the relative trends across the samples are comparable. Figure 8b shows the PDP results for samples 1-5B when loaded, along with the averaged  $E_{corr}$ ,  $i_{corr}$ , and corrosion rate for all five samples which can be seen in Table 2.

**Table 2:** Averaged  $E_{corr}$ ,  $i_{corr}$ , and corrosion rate values for all five samples for unloaded and loaded tests

Sample	Unloaded			Loaded		
	$E_{corr}$ (V)	$i_{corr}$ ( $\mu\text{A}/\text{cm}^2$ )	Corrosion Rate (mpy)	$E_{corr}$ (V)	$i_{corr}$ ( $\mu\text{A}/\text{cm}^2$ )	Corrosion Rate (mpy)
1	-1.30	34	29	-1.30	38	32
2	-1.38	268	230	-1.34	46	39
3	-1.28	54	47	-1.26	126	17
4	-1.33	116	98	-1.33	37	31
5	-1.33	251	206	-1.34	24	20

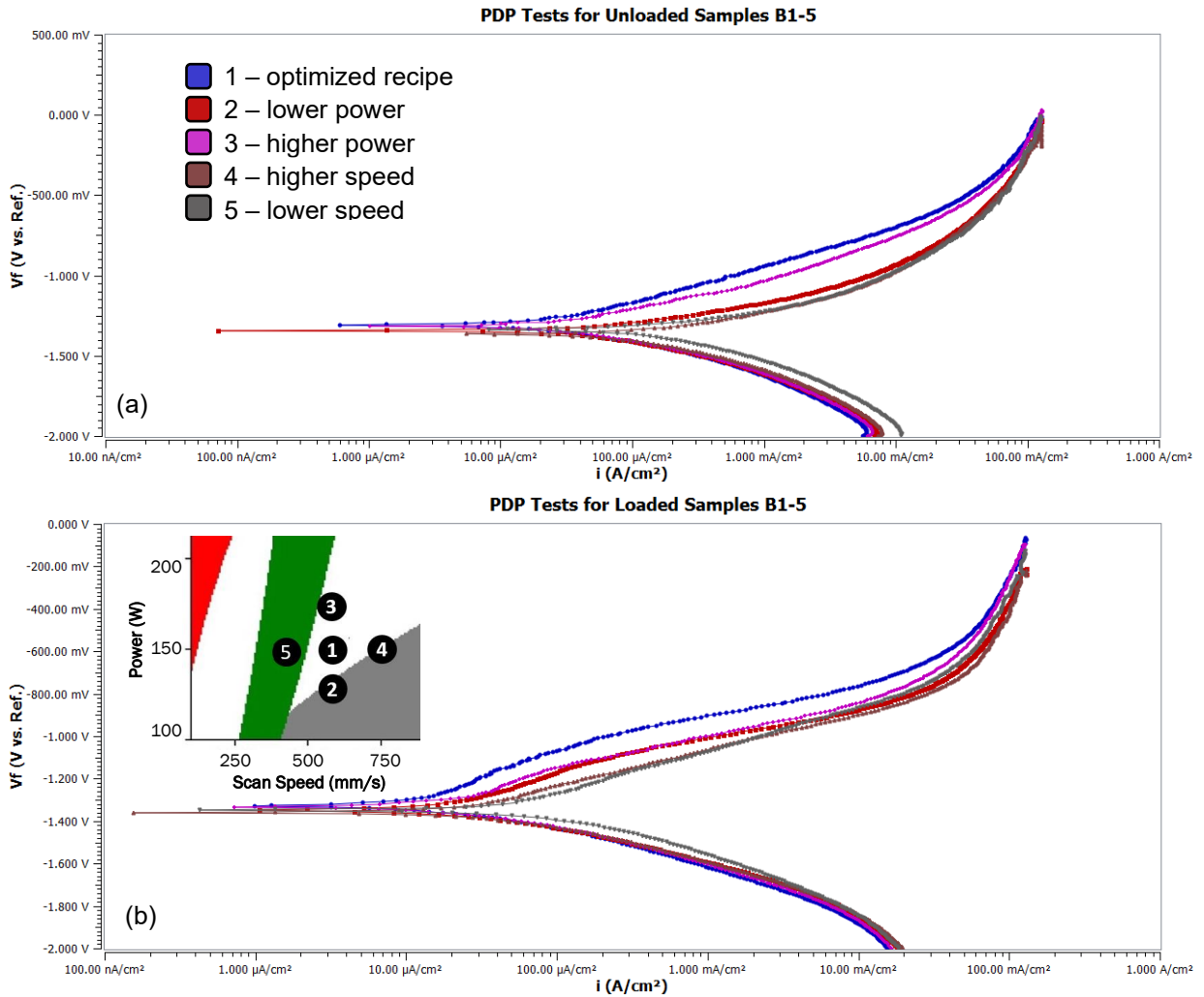


**Figure 8:** Potentiodynamic polarization curves for bottom-layer samples (1–5) under (a) unloaded and (b) loaded conditions. Sample colors: 1B (blue), 2B (red), 3B (pink), 4B, (brown), and 5B (grey).

Based on the hypothesis, the samples were expected to increase  $i_{corr}$  and corrosion rate when it was loaded compared to the unloaded test. Sample 1 supports that hypothesis as the  $i_{corr}$  increased from 34 to 38  $\mu\text{A}/\text{cm}^2$  and the corrosion rate increased from 29 to 32 mpy. As sample 1 was the optimal printing parameters for AZ91 magnesium powder, this was expected; however, this was not the case for samples 2 through 5. As seen in Table 2, the corrosion rate decreased significantly for those samples when loaded during the PDP testing process. Possible explanations include limitations of performing consecutive PDP tests on the same sample in the same solution, which may obscure differences between conditions, as well as increased porosity or reduced energy density in certain parameter sets that could cause non-uniform stress redistribution and influence corrosion behavior. Overall, the range in differences for the parameters of scan speed and laser power might have been too large to obtain the most optimal parameters to see the lowest corrosion rates when a load was induced. Future testing should lower the range of scan speed or laser power from the optimal settings in sample 1 to see changes regarding corrosion within AZ91.

#### 4.4 Effect of Build Height on Corrosion Behavior

Table 3 shows the PDP tests for the three different heights regarding the top, middle, and bottom layers for unloaded and loaded samples. All layers decreased their corrosion from unloaded testing compared to loaded testing. This was due to samples 2-5 having a majority impact on the values leading to the average results for build height regions. The top layers had the highest corrosion rates for both unloaded and loaded testing having values of 169 and 38 mpy, respectively. The bottom layer had the lowest corrosion rates for both unloaded and loaded testing with values of 67 and 12 mpy, respectively, which was expected based on the hypothesis. The bottom layer experiences a different thermal history and thus resulting microstructure that exhibited a lower corrosion rate compared to regions further away from the build plate.

**Table 3 :** Averaged  $E_{corr}$ ,  $i_{corr}$ , and corrosion rate for three regions unloaded and loaded

Sample	Unloaded			Loaded		
	$E_{corr}$ (V)	$i_{corr}$ ( $\mu\text{A}/\text{cm}^2$ )	Corrosion Rate (mpy)	$E_{corr}$ (V)	$i_{corr}$ ( $\mu\text{A}/\text{cm}^2$ )	Corrosion Rate (mpy)
Top	-1.32	204	169	-1.28	45	38
Middle	-1.32	153	131	-1.31	42	35
Bottom	-1.33	79	67	-1.34	14	12

## 5. Discussion

Based on the results, the hypothesis was partially proven as the optimal print parameters did lead to a marginal increase in corrosion rate when a load was induced. In the context of previous studies, this study led to a refinement in the optimal zone for printing as previous theoretical data for the optimal zone showed worse results than the experimental optimal zone. The corrosion rate for samples 2-5 was lower under tension. This unexpected finding may be due to several factors, including porosity morphology or reduced energy density, which could alter how stress is redistributed during corrosion. Future testing should account for this and refine varying the

parameters to a smaller amount to further pinpoint the best parameters needed for stress-corrosion behavior.

There were some limitations to the research that would need to be done in future testing. Primarily, porosity was a vital reasoning for the hypothesis, and the study researched the porosity of how changing the parameters and the regional porosity, but porosity itself was not tested for quantitative data for the samples, so validation in these values should be done. In addition, it was only possible to test the middle of each sample due to the way the sample needed to be tensioned leaving only the middle area able to be evaluated. Research shows the left and right sides of a piece also having different corrosion values on a given sample compared to the middle so future testing would need to be done for this as well. Lastly, the team was only able to test each sample once due to availability and access to MMRL and the AZ91 powder, meaning that once fully trained on how to test the samples, each sample was only tested once for unloaded and loaded data. One sample was polished to test again; however, with the time constraints and the difference in surface area, this was the only one that could be tested this way.

## 6. Summary & Conclusions

This study explored the stress-corrosion behavior of L-PBF AZ91 Mg alloy by varying print parameters. OCP and PDP tests were conducted and analyzed through a Tafel fit method to understand the corrosion performance of the samples. The study found that some samples corrosion rate increased under tension. However, most of the samples corroded more when unloaded which can highlight inaccuracies in the study and requires further testing. Samples closer to the build plate also showed lower corrosion rates likely due to different thermal histories and resulting microstructures. Optical microscopy was not conducted in this study but is recommended to quantitatively understand the different porosity in each sample.

- Corrosion rate under tension increased under ideal print parameters and decreased under suboptimal parameters
- Samples closer to the build plate exhibited a **decreased** corrosion rate
- Changes in laser power and scan speed **increased** corrosion rates (hypothesis supported)

Future work is needed to investigate why tensioned samples for suboptimal parameters exhibited improved corrosion resistance. Optical microscopy is needed to quantify defects driving corrosion such as lack-of-fusion pores and under-melting. Also, further testing is needed to identify parameters that consistently achieve optimized corrosion rates for various industries.

### Acknowledgements

A special thank you to Dr. Michael Sealy for the opportunity to learn and understand additive manufacturing and enabling the ability to go through a research project in a constructive and timely manner in an additive manufacturing research course. Nikhil Patel and Scott Fernander were also a great help for the experiment training, understanding the process for the research plan, and being able to answer questions when the data was difficult to comprehend. Another huge thank you to Ed Yother, the manufacturing technician at the Manufacturing and Materials Research Lab

(MMRL) that was able to help a printing plan for the varied parameters of the AZ91 LBPF printing process. Financial support was provided by the School of Mechanical Engineering at Purdue University in a deep dive research course on additive manufacturing as well as NSF CMMI: 1846478 (rev. 2318705) titled, “CAREER: Hierarchical Structure Integrity of Magnesium Alloys via Asynchronous Laser and Additive Processing.”

### References

- [1] Song, G., Atrens, A., 2004. Understanding Magnesium Corrosion—A Framework for Improved Alloy Performance, *Advanced Engineering Materials*, 5(12), p. 837-858. <https://doi.org/10.1002/adem.200310405>
- [2] Sealy, M. P., Karunakaran, R., Ortgies, S., Madireddy, G., Malshe, A. P., and Rajurkar, K.P., 2021. Reducing corrosion of additive manufactured magnesium alloys by interlayer ultrasonic peening. *CIRP Annals*, 70(1), p. 179-182. DOI: 10.1016/j.cirp.2021.04.052
- [3] Wegner, N., Kotzem, D., Wessarges, Y., Emminghaus, N., Hoff, C., Tenkamp, J., Hermsdorf, J., Overmeyer, L., Walther, F., 2019. Corrosion and Corrosion Fatigue Properties of Additively Manufactured Magnesium Alloy WE43 in Comparison to Titanium Alloy Ti-6Al-4V in Physiological Environment, *Materials*, 12(18), 2892. <https://doi.org/10.3390/ma12182892>
- [4] Zhao, P., Wu, W., Ma, Z. and Dan, Y., 2022. *In situ* study on the effect of stress on corrosion behavior of AZ91 magnesium alloy, *Anti-Corrosion Methods and Materials*, Vol. 69 No. 2, pp. 204-213. <https://doi.org/10.1108/ACMM-09-2021-2542>
- [5] ASTM International, 2019. Standard Practice for Preparation and Use of Direct Tension Stress-Corrosion Test Specimens, *ASTM G49-85*. DOI: 10.1520/G0049-85R19
- [6] Kirkland, N.T., Birbilis, N., Staiger, M.P., 2011. Assessing the corrosion of biodegradable magnesium implants: A critical review of current methodologies and their limitations, *Acta Biomaterialia*, 7(12), p. 4019-4032. DOI: 10.1016/j.actbio.2011.11.014